ACS Partner Journal

CHEM & BIO ENGINEERING

pubs.acs.org/ChemBioEng

Article

Development of Heterometallic Annular Tetranuclear Clusters in Metal−Organic Frameworks for Methane Purification and Storage

Published as part of Chem & Bio Engineering virtual special issue "Advanced Separation Materials and Processes".

Jiao Lei,[#] Zhang-Lei Zhong,[#] Wenyu Yuan, Peng Zhang, Ying Wang, and Quan-Guo Zhai*

Cite This: *Chem Bio Eng.* 2024, 1, 773−782

Read Online

ACCESS | Metrics & More | Article Recommendations | Supporting Information

ABSTRACT: Annular tetranuclear cluster based metal−organic frameworks (MOFs) have displayed unique advantages in gas adsorption and separation due to their highly connected robust architectures. Herein, two novel heterometallic tetranuclear motifs, $[Y_2Cd_2(\mu_3\text{-}O)_2(COO)_8(H_2O)_2]$ and $[Y_2In_2(\mu_3\text{-}O)_2(\mu_2\text{-}O)_2(COO)_8(H_2O)_2]$, were successfully explored, which were further extended by 1,3,5-tris(4-carboxyphenyl)benzene (H_3BTB) tritopic linker to give isostructural MOFs (SNNU-326 and -327). SNNU-326 and -327 both exhibit the abilities to remove impurities (C_2-hydrocarbons and CO_2) in natural gas (NG) and excellent CH_4 storage capacities at high pressures. SNNU-326 shows better CH_4 purification and storage performance than SNNU-327 owing to different framework charges, in which only one counter ion is needed in SNNU-326 but two of them are necessary for SNNU-327, thus resulting in an obvious decrease of surface area. Dynamic breakthrough experiments demonstrate that SNNU-326 can effectively separate CH_4 from equimolar C_2H_2/CH_4, C_2H_4/CH_4, C_2H_6/CH_4, and CO_2/CH_4 mixtures with breakthrough interval times of about 40.6, 35.1, 54.2, and 10.2 min g^{-1} (273 K, 1 bar, 2 mL min^{-1}), respectively. At the same time, SNNU-326 exhibits excellent CH_4 storage capability with total and working uptakes of 154.3 cm^3 (STP) cm^{-3} (80 bar) and 103.4 cm^3 (STP) cm^{-3} (5−65 bar) at 273 K on account of the collaborative impacts of adequate apertures, high surface areas, and multiple open metal sites.

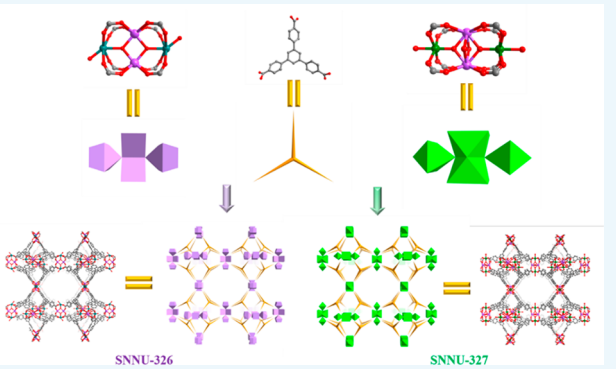

KEYWORDS: *metal−organic framework, annular tetranuclear cluster, methane purification, methane storage, heterometallic cluster, natural gas*

INTRODUCTION

Methane (CH_4), as the primary component of natural gas (NG),[1] is characterized by its (i) high H/C ratios,[2] (ii) high natural abundances,[3] and (iii) high combustion calorific values (55.7 MJ·kg^{-1}), which are comparable to gasoline (46.4 MJ·kg^{-1}).[4] And it has been one of the most important energy sources. However, the utilization rates of CH_4 were affected by the presence of impurities in natural gas, such as CO_2, C_2-hydrocarbons, C_3-hydrocarbons, etc.[5] In addition, it is not economical to use heavy hydrocarbons as fuel directly, which are high-value-added chemical raw materials.[6,7] Therefore, it is necessary to purify CH_4 from NG to improve the combustion efficiency and commercial value. On the other hand, the major disadvantage of CH_4 in transportation is its low energy density.[8] Thus, development of efficient onboard CH_4 storage strategies is critical to make CH_4 a new type of fuel for successful transportation applications. Adsorbed natural gas (ANG) is one of the most effective and feasible methods for storing NG currently, which depends on the characteristics of the porous adsorbents.[9,10]

Compared with traditional porous materials, such as zeolites, activated carbons, etc., metal−organic frameworks (MOFs) have become a potential material for CH_4 storage and purification attributed to their many advantages, such as adjustable structure, high specific surface areas, and easy functionalization.[11−13] Among the large number of MOFs,[14−16] tetranuclear cluster based MOFs exhibit the advantages of high stabilities, devisible structures, and abundant open metal sites (OMSs)[7,17,18] and show potentials in the fields of gas adsorption and separation,[19] catalysis,[20] fluorescence,[21]

Received: January 8, 2024
Revised: February 14, 2024
Accepted: March 10, 2024
Published: March 15, 2024

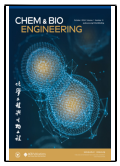

https://doi.org/10.1021/cbe.4c00009
Chem Bio Eng. 2024, 1, 773−782

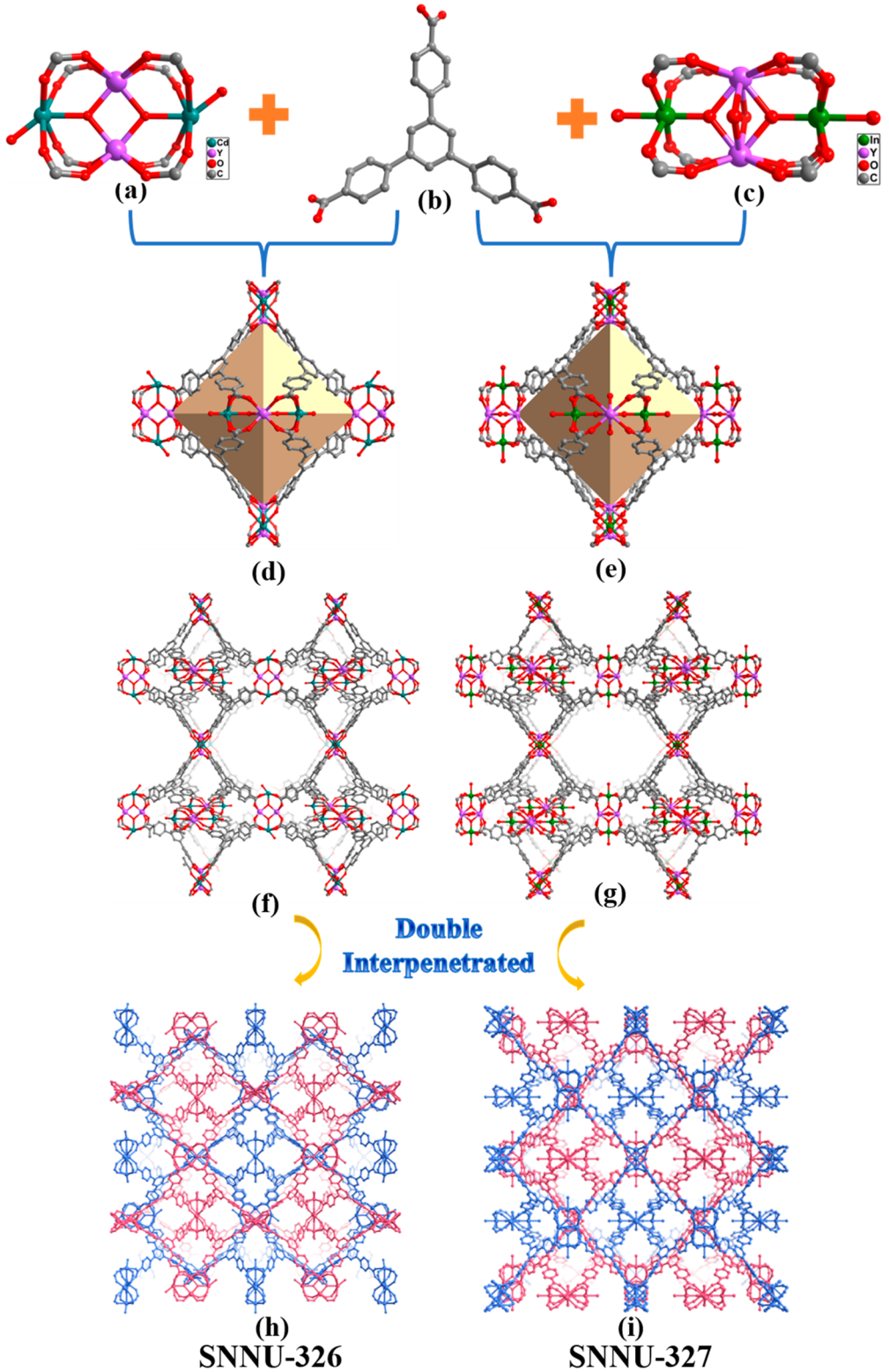

Figure 1. (a) $[Y_2Cd_2]$ tetranuclear cluster in SNNU-326; (b) the BTB ligand; (c) $[Y_2In_2]$ tetranuclear cluster in SNNU-327; (d, e) the octahedral cages of SNNU-326 and -327; (f, g) 3D structures of SNNU-326 and -327; (h, i) the double interpenetrated structures of SNNU-326 and -327.

etc. The common tetranuclears secondly building blocks (SBUs) include the 6-c $[Zn_4O(COO)_6]$ tetrahedral cluster in the classical MOF-5,[22,23] the 8-c $[Co_4(\mu_4\text{-}O)(COO)_8]$ annular cluster in PCN-9 (Co),[24] the $[M_4(\mu_3\text{-}O)_2(COO)_8]$ cluster,[25] the tetrahedral M_4X_4 (X = halogens) cluster,[26,27] and the linear 4-c $[In_4O_2(COO)_4]$[28] cluster with each O atom bridging three metal centers, etc. In addition, some rare tetranuclear clusters are included, such as Hou et al. reported the $[M_4O(COO)_3(NN)_3]$[29] cluster, a variant of the 6-c $[M_4O(COO)_6]$ cluster, where three-coordinated carboxylic acid groups are replaced by pyrazole groups. In addition, some tetranuclear clusters with different numbers of pyrazole groups replacing the

https://doi.org/10.1021/cbe.4c00009
Chem Bio Eng. 2024, 1, 773−782

carboxyl group are reported, such as the $[Zn_4(\mu_4\text{-}O)(COO)_2(pz)_4]$[30] (pz: pyrazine) cluster and the $[Co_4(\mu_4\text{-}O)(pz)_6]$[31] cluster.

To synthesize the novel annular tetranuclear cluster, heterometal strategies are useful because different metal ions always show different coordination modes and may produce rare connection styles. In addition, metal ions with different valence charges will make the framework represent different charged properties and then infect the gas adsorption and separation performance of the frameworks. Based on the above situation, two novel heterometallic annular tetranuclear cluster based MOFs (SNNU-326 and -327) were synthesized based on the heterometal strategy with the same organic ligand (H_3BTB: 1,3,5-tris(4-carboxyphenyl)benzene). And two types of mixed metal annular tetranuclear cluster are observed: $[Y_2Cd_2(\mu_3\text{-}O)_2(COO)_8(H_2O)_2]$ in SNNU-326 formed through Cd^{2+} and Y^{3+} ions and $[Y_2In_2(\mu_3\text{-}O)_2(\mu_2\text{-}O)_2(COO)_8(H_2O)_2]$ in SNNU-327 formed by In^{3+} and Y^{3+} ions. With the synergistic effect of high surface area, suitable pore size, and multiple OMSs, SNNU-326- and -327 not only show remarkable CH_4 purification property from CO_2/CH_4 and C_2-hydrocarbons/CH_4 mixtures but also show CH_4 storage capabilities at high pressure.

EXPERIMENTAL SECTION

Synthesis. *[YCd(μ_3-O)(BTB)$_{4/3}$(H_2O)(DMAM)] (SNNU-326).* The raw materials $Y(NO_3)_3{\cdot}6H_2O$ (0.016 g, 0.04 mmol), $Cd(NO_3)_2{\cdot}4H_2O$ (0.040 g, 0.13 mmol), H_3BTB (0.024 g, 0.055 mmol), 2-FBA (0.240 g, 1.70 mmol), 6 mL of DMF, and 0.9 mL of H_2O were mixed in a 20 mL glass vial. The sealed mixed solution was ultrasound to dissolution and then transferred to a 90 °C oven for 4 days. The colorless block crystals were gained upon cooling to room temperature. After washing with methanol, the yield was about 63% based on H_3BTB.

[YIn(μ_3-O)(μ_2-O)(BTB)$_{4/3}$(H_2O)(DMAM)$_2$] (SNNU-327). The raw materials $Y(NO_3)_3{\cdot}6H_2O$ (0.016 g, 0.04 mmol), $In(NO_3)_3{\cdot}xH_2O$ (0.040 g, 0.13 mmol), H_3BTB (0.024 g, 0.055 mmol), 2-FBA (0.173 g, 1.23 mmol), 6 mL of DMF, and 0.9 mL of H_2O were mixed in a 20 mL glass vial. The sealed mixed solution was ultrasound to dissolution and then transferred to a 90 °C oven for 4 days. The colorless block crystals were gained upon cooling to room temperature. After washing with methanol, the yield was about 65% based on H_3BTB.

Low Pressure Gas Adsorption. For the purpose of exploring the permanent porosity of SNNU-326 and SNNU-327, N_2 adsorption and desorption isotherms at 77 K were collected by a Micromeritics 3Flex analyzer. Before measurement, SNNU-326 and SNNU-327 were activated through CH_3OH exchange for 3 days and heated for 10 h at 100 °C. The adsorption and desorption isotherms with activated samples of single component CO_2, C_2H_2, C_2H_4, C_2H_6, and CH_4 at 1 atm were conducted at 273, 283, and 298 K.

High-Pressure Methane Adsorption. The adsorption isotherms for methane at high pressure were conducted at 273 and 298 K with an activated sample to evaluate the CH_4 storage performance. Ultrapure CH_4 and He (99.999% purity) gases were used for the high-pressure adsorption experiments. The high-pressure CH_4 adsorption was carried out with a BSD high-pressure analyzer.

Dynamic Breakthrough Experiments. The breakthrough experiments were conducted on a self-built instrument, which mainly consisted of three units including a distribution unit, through column element, and analytical detection unit. The activated MOF samples (SNNU-326, 0.50 g; SNNU-327, 0.46 g) were packed into a stainless-steel column with an internal diameter of about 4.0 mm and an outer diameter of about 6.0 mm, respectively. Then, the packed column was first swept with He gases at a rate of 30 mL min^{-1} for 30 min at room temperature to further activate the sample before the measurements, and the pressure of sweeping was often 2 bar. In addition, the testing temperature was maintained by manipulating the water bath circulating device.

After sweeping, the on-line gas mass spectrometry analyzer with an HPR-20 R&D model to online testing was linked to the column, with adjusting the flow of helium to the total test flow for stabilizing the gas flow of gas line before being switched to the adsorbent column. The flow of He was then turned off, while the 50:50 (v/v) gas mixture of CO_2/CH_4, C_2H_2/CH_4, C_2H_4/CH_4, and C_2H_6/CH_4 was allowed to feed into the column.

RESULTS AND DISCUSSION

It is noted that the heterometallic strategy has been demonstrated as a versatile route for the design of polynuclear metal clusters in MOFs; however, it has rarely been reported for annular tetranuclear motifs up to now. In this work, Y^{3+} together with Cd^{2+} or In^{3+} ions were mixed to assemble with H_3BTB through a one-pot solvothermal reaction, and two novel heterometallic MOFs (SNNU-326 and -327) with two types of annular tetranuclear clusters were obtained. SNNU-326 and SNNU-327 both crystallize in the cubic $Im\bar{3}$ space group and exhibit isostructuralism consisting of triangular tricarboxylate ligand (H_3BTB) and heterometallic annular tetranuclear clusters $[Y_2Cd_2(\mu_3\text{-}O)_2(COO)_8(H_2O)_2]$ and $[Y_2In_2(\mu_3\text{-}O)_2(\mu_2\text{-}O)_2(COO)_8(H_2O)_2]$ for SNNU-326 and SNNU-327, respectively. Both of them show 3,8-c three-dimensional frameworks, in which the deprotonated H_3BTB ligands are conducted as the 3-c nodes to connect three SBUs, and the SBU acts as 8-c nodes to connect eight BTB ligands. From the topological point of view, the overall framework of SNNU-326 and -327 shows a completely 3,8-connected network with a point symbol of $\{4^3\}_8\{4^8{\cdot}6^4{\cdot}8^{12}{\cdot}10^4\}_3$.

The asymmetric unit of SNNU-326 consists of one Y^{3+}, one Cd^{2+}, one μ_3-O atom, 1/3 BTB ligand, and one terminal H_2O molecule (Figure S1a). It is worth noting that the SNNU-326 structure is highly disordered, in which both the BTB ligand and the terminal H_2O molecule are double disordered (Figure S1b). Each Cd^{2+} is six-coordinated with one μ_3-O atom, four carboxyl O atoms from four BTB ligands, and one terminal H_2O molecule. Each Y^{3+} center is also in the six-coordination mode, which coordinated with two μ_3-O atoms and four carboxyl O atoms from four BTB ligands. The $[Y_2Cd_2(\mu_3\text{-}O)_2(COO)_8(H_2O)_2]$ building blocks in SNNU-326 are shown in Figure 1a, and each metal ion is connected by a μ_3-O atom. The asymmetric unit of SNNU-327 consists of one Y^{3+}, one In^{3+}, 1/3 BTB ligand, one μ_3-O atom (O2), one μ_2-O atom (O3), and one terminal H_2O molecule (O1) (Figure S3). Each Y^{3+} form a novel eight-coordinated configuration with four carboxyl O atoms from four BTB ligands, two μ_3-O atoms, and two μ_2-O atoms. Each In^{3+} is a classical octahedral six-coordination configuration, which coordinates with four carboxyl O atoms from four ligands, one μ_3-O atom, and one terminal H_2O molecule. The SBU $[Y_2In_2(\mu_3\text{-}O)_2(\mu_2\text{-}O)_2(COO)_8(H_2O)_2]$ of SNNU-327 was shown in Figure 1c. And the major difference of SBU from SNNU-326 is the coordination mode of Y^{3+}, which is eight-coordination modes in SNNU-327 and six-coordination modes in SNNU-326. SNNU-327 also shows the 3,8-c structure (Figure 1).

Detailed structural analysis shows that SNNU-326 and SNNU-327 are both electronegative frameworks with one and two $DMAM^+$ ions to balance the charge, respectively. The 3D frameworks of SNNU-326 and -327 are both 3,8-c modes constructed by connection of each octahedral cage in vertex to vertex mode, which is composed of six SBUs as the vertex and eight BTB ligands as faces. Among them, the octahedral cage diameters in SNNU-326 and SNNU-327 are 18.8 and 18.6 Å,

https://doi.org/10.1021/cbe.4c00009
Chem Bio Eng. 2024, 1, 773−782

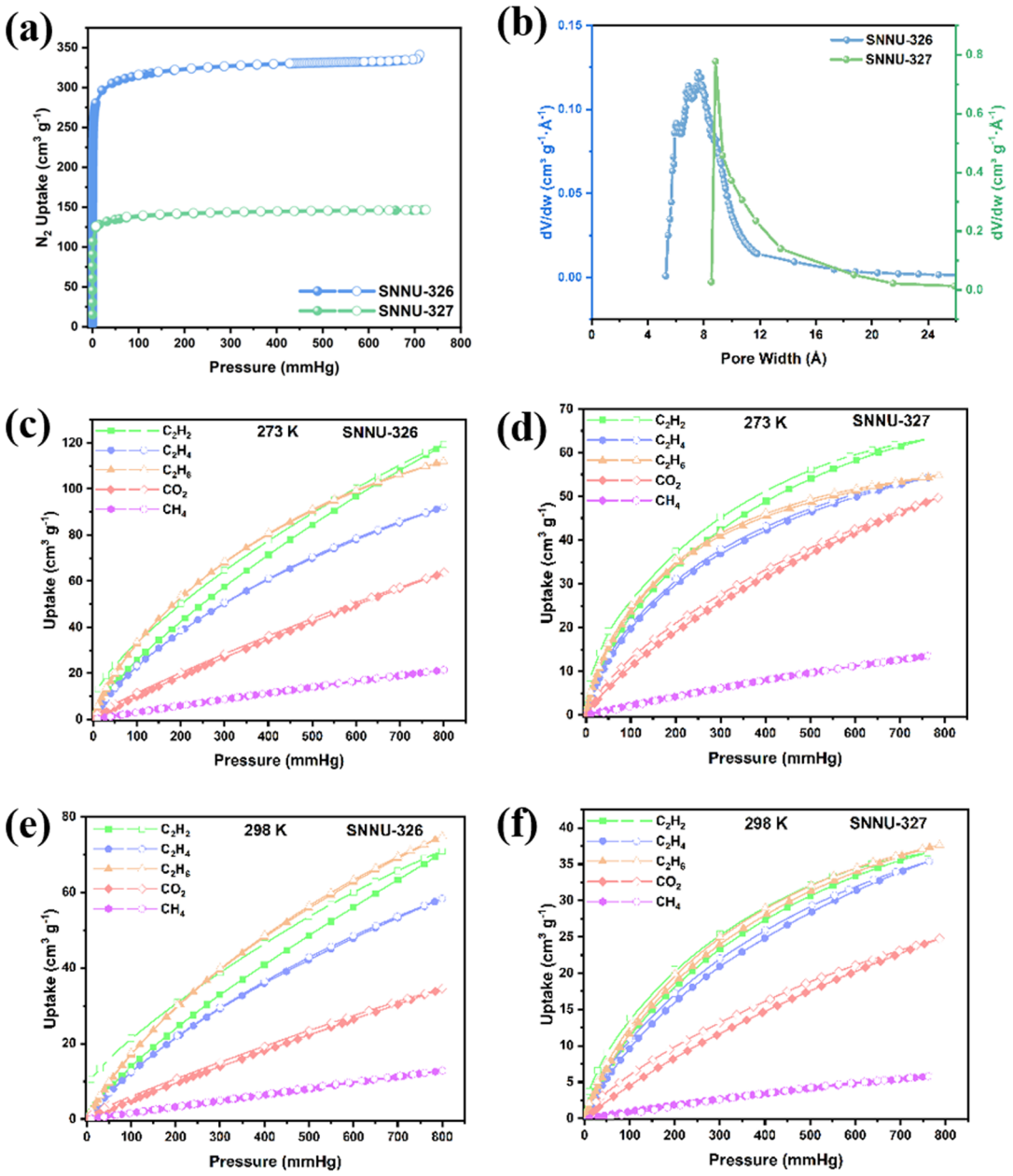

Figure 2. N_2 adsorption and desorption isotherms (a) and pore width distributions (b) of SNNU-326 and -327. The adsorption and desorption isotherms of C_2H_2, C_2H_4, C_2H_6, CO_2, and CH_4 at 273 K (c, d) and 298 K (e, f) for SNNU-326 and -327.

and the four octahedral cages on the same plane are connected to form one-dimensional irregular hexagonal channels with diameters of about 21.4 × 14 and 19.6 × 11.6 Å^2, respectively. The small difference in the one-dimensional channel size is caused by the difference in the size of the two metal clusters. Owing to the large size of the BTB ligands, SNNU-326 and SNNU-327 form large size octahedral cages and one-dimensional channels and thus construct a double interpenetrated structure along the [110] direction (Figure 1h,i). SNNU-326 and SNNU-327 have the same connection modes but completely different inorganic SBUs, which demonstrates the diversity of MOF structures.

As shown in Figure S5, the experimental powder X-ray diffraction (PXRD) patterns of the synthesized sample, after solvent exchange, and after the adsorption test of the compounds SNNU-326 and -327 are consistent with the simulation spectra of single crystal data, which proves the purity and high crystallinity of SNNU-326 and -327, and the frameworks remain stable after adsorption experiments. In addition, the thermogravimetric analysis (TGA) curves shown in Figure S6 exhibit that SNNU-326 can be stabilized to ca. 430 °C. When the temperature continues to rise, the weight significantly decreases and the framework begins to collapse. Compared with SNNU-326, the thermal stability of SNNU-327 is reduced. It can be stabilized to about 370 °C.

The porosities of SNNU-326 and -327 are calculated by Platon according to the single crystal data. The results show that the porosities of SNNU-326 and -327 are 53.4% (10596.3 Å^3/19859.6 Å^3) and 59.5% (11459.6 Å^3/19252.5 Å^3), respectively. As shown in Figure 2a, the N_2 adsorption isotherms at 77 K of SNNU-326 and -327 exhibit the obvious type I adsorption behavior and the saturated adsorption capacities at 1 atm are

https://doi.org/10.1021/cbe.4c00009
Chem Bio Eng. 2024, 1, 773−782

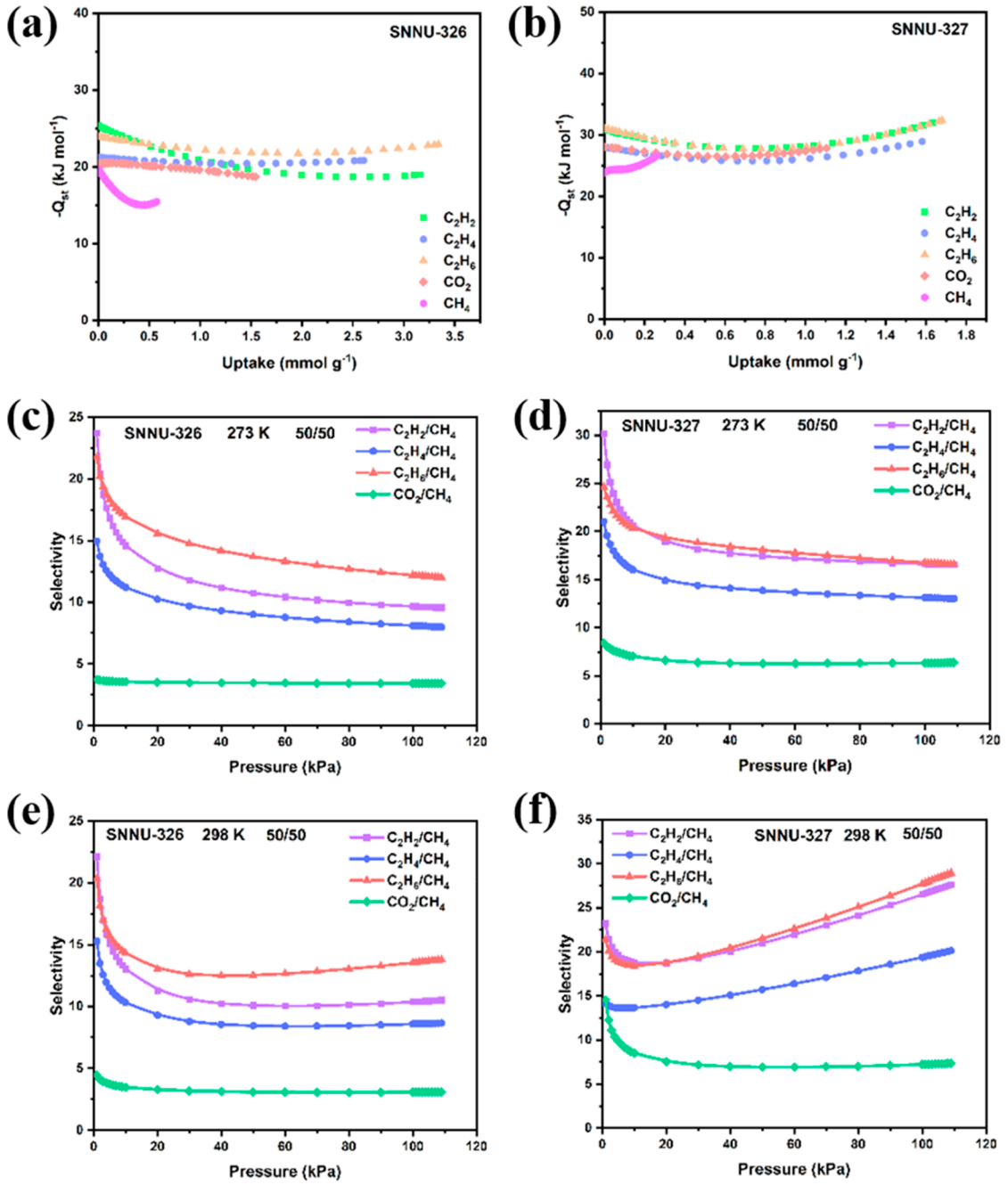

Figure 3. Isosteric heats of adsorption ($-Q_{st}$) (a, b) and IAST selectivities calculated at 273 K (c, d) and 298 K (e, f) for SNNU-326 and -327.

341.3 and 146.7 cm^3 g^{-1}, respectively. The Brunauer−Emmet−Teller (BET) and Langmuir specific surface areas of SNNU-326 and -327 are 1233 and 1362 m^2 g^{-1} and 538 and 597 m^2 g^{-1}, respectively, based on the N_2 adsorptions. The apparent reduction of surface areas of SNNU-327 can be attributed to the further trapped counter ions in the framework. The distinct pore size decrease compared with the single crystal data can be a result of the double interpenetrating structures.

Considering the high porosities, suitable pore size, and multiple OMSs of SNNU-326 and -327, the adsorption properties of C_2H_2, C_2H_4, C_2H_6, CO_2, and CH_4 are further tested at 273, 283, and 298 K (Figure 2 and Figure S7). For SNNU-326, at 273 K and 1 atm, the adsorption capacities of C_2H_2, C_2H_4, C_2H_6, CO_2, and CH_4 are 116.2, 89.9, 109.9, 62.3, and 20.6 cm^3 g^{-1}, respectively (Figure 2c). As the temperature increases to 283 and 298 K, the adsorption capacities decrease because the adsorptions have endothermic behavior. For SNNU-327, at 273 K and 1 atm, the adsorption capacities of C_2H_2, C_2H_4, C_2H_6, CO_2, and CH_4 are 63.0, 54.1, 54.5, 48.6, and 13.2 cm^3 g^{-1}, respectively (Figure 2d). Similarly, as the temperature increases, the adsorption capacities of C_2H_2, C_2H_4, C_2H_6, CO_2, and CH_4 are decreased (Tables S2 and S3).

The adsorption capacities of SNNU-327 decrease significantly compared with SNNU-326 although they are isostructural structures. The difference may be mainly caused by the electronegativity of the framework. As mentioned above, the framework of SNNU-327 has two units of negative charge, thus requiring two DMAM$^+$ ions to balance the charges. However, SNNU-326 only needs one DMAM$^+$ to balance the charges. Thus, the pores of SNNU-327 are occupied by much more

https://doi.org/10.1021/cbe.4c00009
Chem Bio Eng. 2024, 1, 773−782

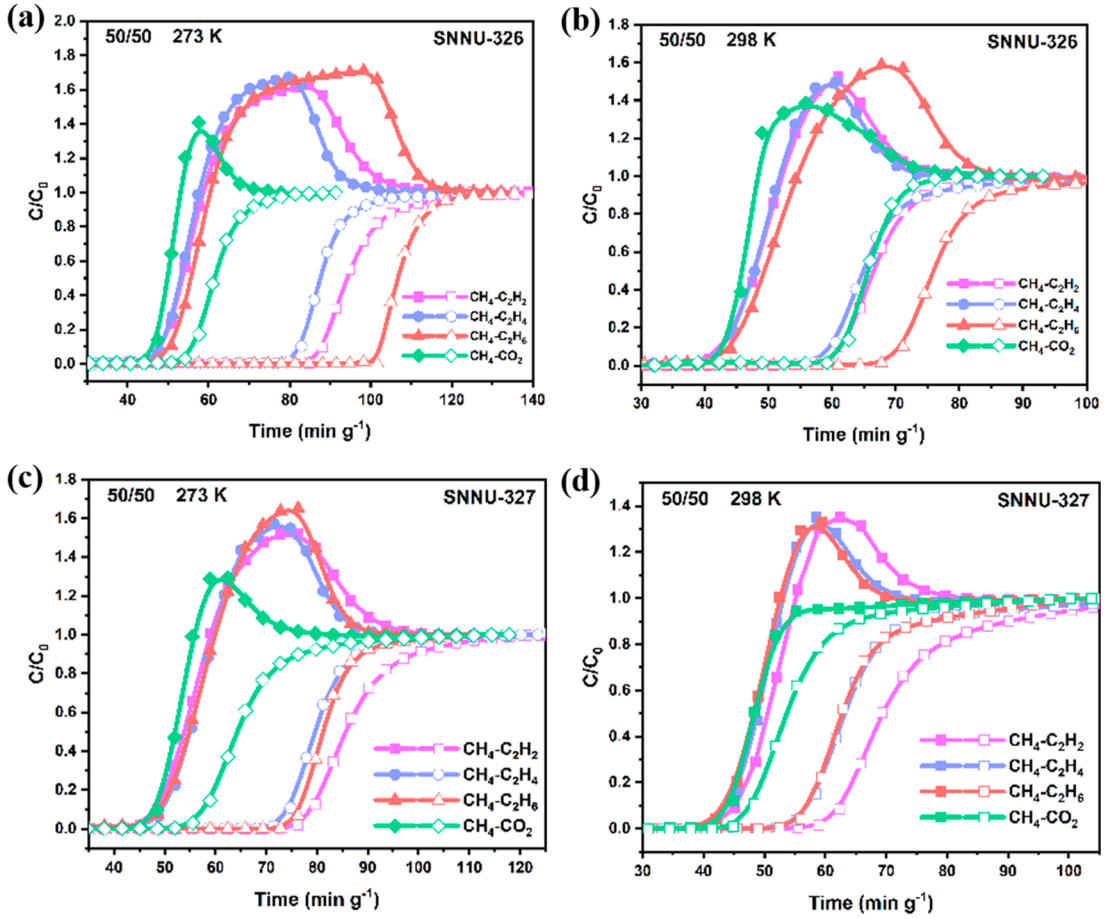

Figure 4. Experimental breakthrough curves of SNNU-326 and -327 for C_2H_2/CH_4, C_2H_4/CH_4, C_2H_6/CH_4, and CO_2/CH_4 (50/50, total flow rate 2 mL min^{-1}) mixed gases at 273 K (a, c) and 298 K (b, d).

$DMAM^+$ and the interaction sites are decreased accordingly, resulting in a significant decrease in adsorption capacity.

To further understand the interaction between the frameworks and gas molecules, the adsorption heat ($-Q_{st}$) of each component gas was calculated by fitting the adsorption curves of single component gas of SNNU-326 and -327 at 273, 283, and 298 K by virial model. The results show that the $-Q_{st}$ values at zero loading of C_2H_2, C_2H_4, C_2H_6, CO_2, and CH_4 are 25.4, 21.2, 23.9, 20.3, and 19.7 kJ mol^{-1} for SNNU-326, and 30.8, 28.0, 31.1, 28.1, and 23.9 kJ mol^{-1} for SNNU-327, respectively (Figure 3a,b). The lowest $-Q_{st}$ values for CH_4 compared with other gases of SNNU-326 and -327 prove that the interactions between SNNU-326 and -327 frameworks and CH_4 molecules are weaker than those of other gases. Therefore, they exhibit the potential in thermodynamics to purify CH_4 from C_2-hydrocarbon/CH_4 and CO_2/CH_4 mixtures.

The selectivities were calculated based on the ideal adsorbed solution theory (IAST) by fitting the experimental gas adsorption isotherms through the dual-site Langmuir−Freundlich (DSLF) equations. As shown in Figure 3 and Figure S8, SNNU-326 and -327 both exhibit high IAST selectivities for C_2-hydrocarbon/CH_4 and CO_2/CH_4 at 273, 283, and 298 K. Specifically, the IAST selectivities for C_2H_2/CH_4, C_2H_4/CH_4, C_2H_6/CH_4, and CO_2/CH_4 (50/50) of SNNU-326 are 23.7−9.6, 15.0−8.0, 21.7−12.0, and 3.7−3.5, respectively, at 273 K and 0−1 bar. Under the same conditions, the values for SNNU-327 are 30.1−16.5, 21.0−13.0, 24.7−16.6, and 8.4−6.4, respectively (Table S4−S5). The IAST selectivities provide theoretical support to purify CH_4 from C_2-hydrocarbon/CH_4 and CO_2/CH_4 mixtures for SNNU-326 and -327. Besides, the CO_2/CH_4 selectivity at 298 K (14.5−7.3) of SNNU-327 has surpassed some famous MOF adsorbents, such as ZJU-16 (8−3.6),[32] ZIF-78 (~11),[33] [Cu(bpy-1)$_2$(SiF_6)] (~9−10.5),[34] and HKUST-1 (~4−7).[35]

Based on the above results of adsorption isotherms, $-Q_{st}$ values and IAST selectivities, the practical CH_4 purification performances of SNNU-326 and -327 were further tested through fixed bed breakthrough experiments at 273 and 298 K (Figure 4, Tables S6 and S7). The activated SNNU-326 and -327 were loaded into the steel sample tube and purged with 30 mL min^{-1} He gas for 30 min at ambient temperature and pressure. After that, the equimolar mixed gases were injected into the sample tube with a flow rate of 2 mL/min and detected by a chromatograph. As shown in Figure 4, SNNU-326 and -327 can purify CH_4 from the C_2-hydrocarbon/CH_4 and CO_2/CH_4 (v/v = 50/50) mixtures and CH_4 outflows firstly. Among these, the breakthrough interval times for C_2H_2/CH_4, C_2H_4/CH_4, C_2H_6/CH_4, and CO_2/CH_4 of SNNU-326 at 273 K are about 40.6, 35.1, 54.2, and 10.2 min g^{-1}, respectively, which are comparable with some well-known MOF adsorbent materials, such as ZJNU-59[36] (~7.6 min for C_2H_2/CH_4 = 50/50 (v/v) and ~2.6 min for CO_2/CH_4 = 50/50 (v/v) at 298 K and 1 bar), NbU-9-NH_2[37] (26 min for C_2H_2/CH_4 = 50/50 (v/v, 3 mL/min flow rate) at 273 K and 1 bar), and InOF-1[38] (~6 min for C_2H_6/CH_4 = 50/50 (v/v, 5 N mL/min flow rate) at 298 K and 100 kPa). Notably, SNNU-327 also shows excellent CH_4 purifica-

https://doi.org/10.1021/cbe.4c00009
Chem Bio Eng. 2024, 1, 773−782

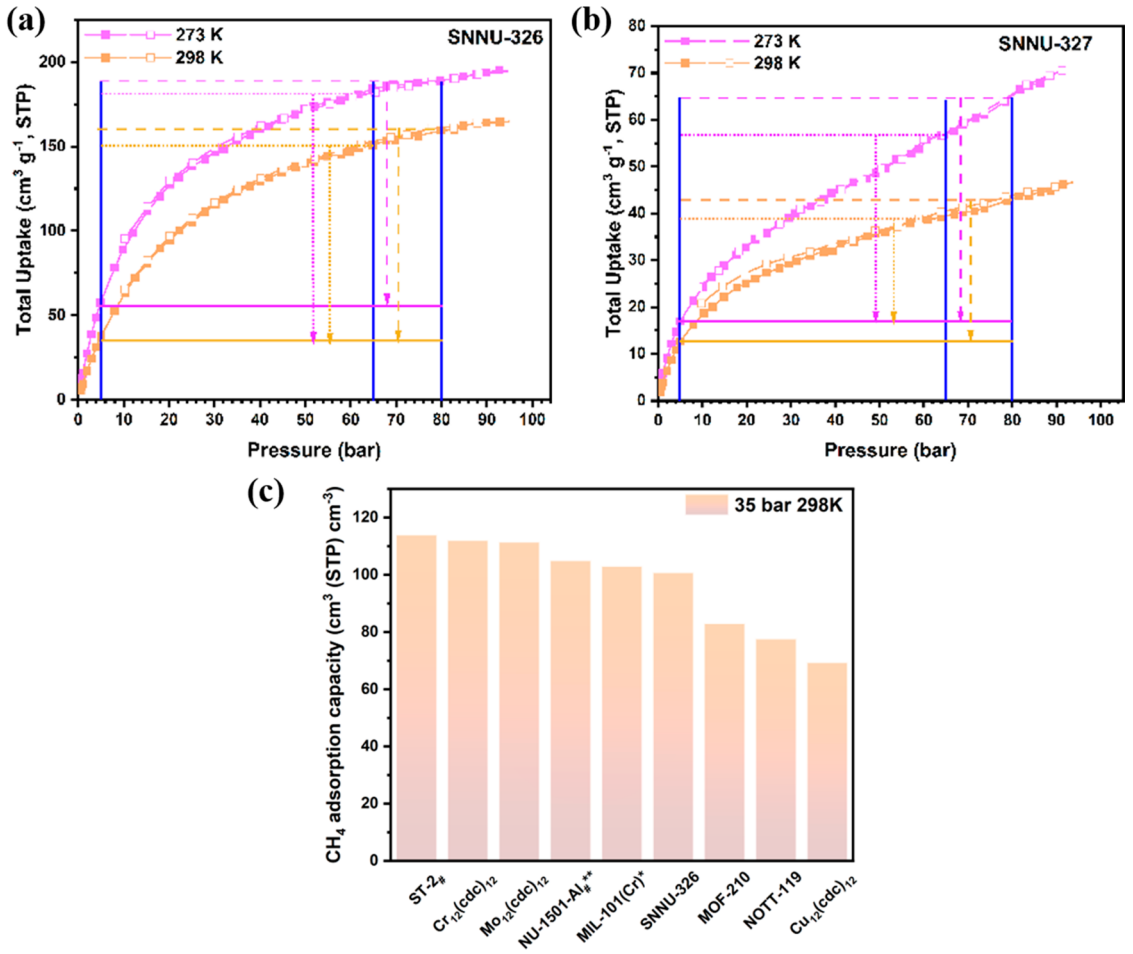

Figure 5. High-pressure CH_4 adsorption and desorption isotherms at 273 and 298 K for SNNU-326 (a) and SNNU-327 (b) and the comparison of CH_4 working capacity of SNNU-326 with the some top CH_4 storage MOF candidates: ST-2 (~114 cm^3 cm^{-3}),[2] $Mo_{12}(cdc)_{12}$ (111.5 cm^3 cm^{-3}), $Cr_{12}(cdc)_{12}$ (112.1 cm^3 cm^{-3}),[10] NU-1501-Al (~105 cm^3 cm^{-3}),[38] MIL-101(Cr) (~103 cm^3 cm^{-3} at 303 K),[39] $Cu_{12}(cdc)_{12}$ (69.4 cm^3 cm^{-3}),[10] NOTT-119 (77.7 cm^3 cm^{-3} of excess uptake),[40] MOF-210 (83 cm^3 cm^{-3}),[41] and at 35 bar (#, estimated; **, 296 K; *, 303 K) (c).

tion performance and the breakthrough interval times at 273 K for C_2H_2/CH_4, C_2H_4/CH_4, C_2H_6/CH_4, and CO_2/CH_4 are ~31.2, 22.7, 27.7, and 6.9 min g^{-1}, respectively. The yield of CH_4 is an important factor in evaluating an adsorbent. For SNNU-326, the yields of CH_4 (purity >99%) from C_2H_2/CH_4, C_2H_4/CH_4, C_2H_6/CH_4, and CO_2/CH_4 breakthrough experiments at 273 K are ~1.81, 1.28, 2.12, and 0.15 mmol g^{-1}, respectively. These values are ~1.39, 1.02, 1.23, and 0.16 mmol g^{-1} for SNNU-327. Obviously, the purification performances for C_2-hydrocarbon/CH_4 are better than CO_2/CH_4 because SNNU-326 and -327 frameworks show more strongly interactions with C_2-hydrocarbons than CO_2.

The high porosities and surface areas, together with the suitable pore sizes make us evaluate the CH_4 storage performance at high pressure of SNNU-326 and -327. As shown in Figure 5, the adsorption capacities of SNNU-326 at 273 and 298 K and 90 bar are 194 and 164 cm^3 (STP) g^{-1}. These values are only 70 and 45 cm^3 (STP) g^{-1} for SNNU-327 under the same conditions. The CH_4 adsorption capacities of SNNU-327 decrease significantly compared with SNNU-326 which can mainly be attributed to the large number of counterions in the frameworks, which occupies the pore spaces.

In addition, the total volume adsorption capacities at 35, 65, and 80 bar are calculated using the crystal density. At 273 K, the total adsorption amounts of SNNU-326 at 35, 65, and 80 bar are 125.8, 150.6, and 154.3 cm^3 (STP) cm^{-3}, respectively. At 298 K, the values decrease to 100.8, 123.5, and 130.5 cm^3 (STP) cm^{-3}. In 1993, the U.S. Department of Energy proposed a key indicator of 35 bar adsorption capacities in order to meet the demand for CH_4 extraction. Notably, the uptakes of SNNU-326 at 35 bar and 298 K are approximate to many well-known MOFs, such as ST-2 (~114 cm^3 cm^{-3}),[2] $Mo_{12}(cdc)_{12}$ (111.5 cm^3 cm^{-3} at 35 bar and 298 K),[10] $Cr_{12}(cdc)_{12}$ (112.1 cm^3 cm^{-3} at 35 bar and 298 K),[10] NU-1501-Al (~105 cm^3 cm^{-3}),[39] and MIL-101(Cr) (~103 cm^3 cm^{-3} at 35 bar and 303 K)[40] and are even superior to some hopeful MOFs, such as $Cu_{12}(cdc)_{12}$ (69.4 cm^3 cm^{-3} at 35 bar and 298 K),[10] NOTT-119 (77.7 cm^3 cm^{-3} of excess uptake at 35 bar and 298 K),[41] and MOF-210 (83 cm^3 cm^{-3} at 35 bar and 298 K)[42] (Figure 5c). The total volume adsorption amounts of SNNU-327 are also lower than that of SNNU-326, which is 27.1, 34.1, and 37.2 cm^3 (STP) cm^{-3} at 298 K and 35, 65, and 80 bar, respectively.

Similarly, since SNNU-326 shows excellent CH_4 adsorption capacities at high pressure, its working capacities under different pressures are calculated (Table S8). At 273 K, the working capacities of SNNU-326 at 5−35, 5−65, and 5−80 bar are 78.6, 103.4, and 107.1 cm^3 (STP) cm^{-3}, respectively. When the temperature increases to 298 K, their values decrease to 70.1, 92.8, and 99.8 cm^3 (STP) cm^{-3}. These values are comparable to some famous MOFs, such as MOF-210 (69 cm^3 cm^{-3} at 35 bar

https://doi.org/10.1021/cbe.4c00009
Chem Bio Eng. 2024, 1, 773−782

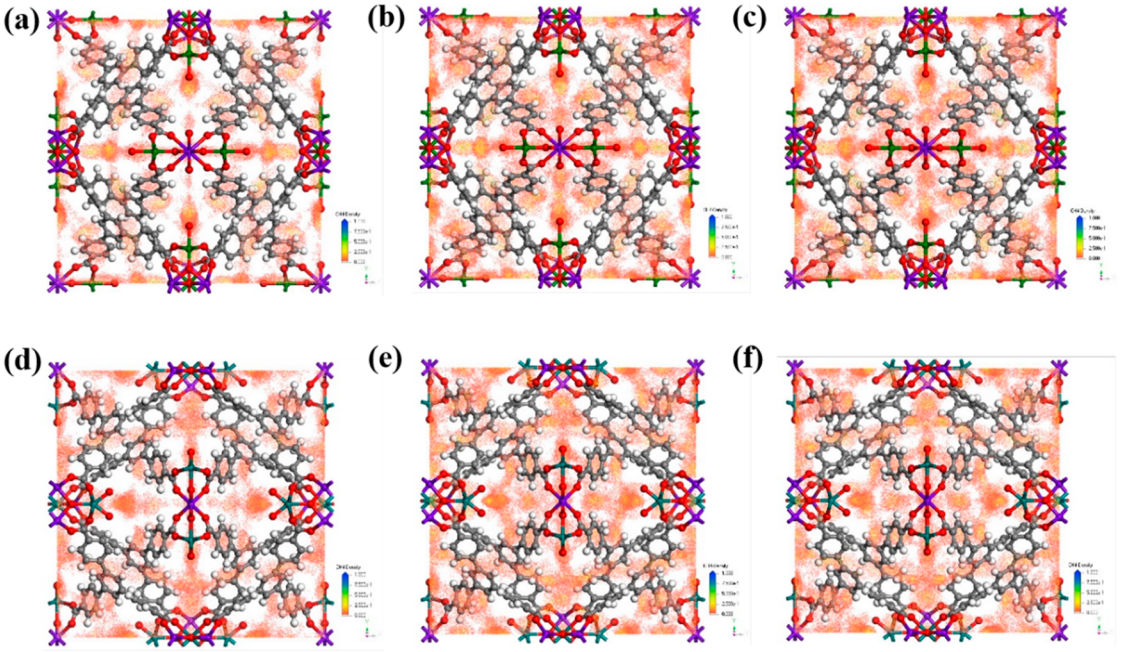

Figure 6. Density distributions of CH_4 simulated by GCMC under 298 K and 5, 65, and 80 bar for SNNU-326 (a–c) and SNNU-327 (d–f).

and 298 K)[40] and UiO-66_B (~80 cm^3 cm^{-3} at 35 bar and 298 K).[5] In a word, SNNU-326 exhibits high CH_4 storage performance under high pressure owing to its suitable pore size, high specific surface area, and multiple OMSs.

In order to further understand the purification and storage mechanism of SNNU-326 and -327, the adsorption sites and density distributions of CH_4 molecules are determined by GCMC simulation. The results show that CH_4 molecules are mainly located near the metal clusters and are adsorbed in the pores through C–H···π interaction with neighboring BTB ligands in SNNU-326 and SNNU-327. As shown in Figure S17a, the CH_4 molecule is adsorbed through two C–H···O hydrogen bonds with the O atoms from carboxyl (the distances are 3.6452 and 3.8065 Å) and one C–H···π (3.0905 Å) with the central benzene ring of the BTB ligand in SNNU-326. As for SNNU-327, the adsorption sites are similar to SNNU-326, in which the CH_4 forms four C–H···O hydrogen bonds with O atoms from carboxyl (3.3026, 3.5573, 3.2636, and 3.3235 Å, respectively) and one C–H···π interaction with the central benzene ring of the ligand with a distance of 3.0293 Å (Figure S17b). In addition, the CH_4 distribution densities at 5, 65, and 80 bar were calculated to understand the storage performance of SNNU-326 and -327. The results show that the CH_4 distribution density shows significant increases with the pressure from 5 to 65 bar and then exhibits a gradually increase from 65 to 80 bar, which are consistent with the experimental results (Figure 6).

CONCLUSION

In summary, two isostructural MOFs (SNNU-326 and -327) are successfully synthesized by the Y^{3+}/Cd^{2+} and Y^{3+}/In^{3+} heterometallic combinations, which contain novel $[Y_2Cd_2(\mu_3\text{-}O)_2(COO)_8(H_2O)_2]$ and $[Y_2In_2(\mu_3\text{-}O)_2(\mu_2\text{-}O)_2(COO)_8(H_2O)_2]$ annular tetranuclear clusters, respectively. Thanks to the suitable pore size and high surface areas and porosities, together with multiple OMSs, SNNU-326 and -327 exhibit not only remarkable purification ability of CH_4 from C_2-hydrocarbons/CH_4 and CO_2/CH_4 mixtures but also excellent CH_4 storage capacity at high pressure. Regulated by the framework charge, SNNU-326 shows better CH_4 purification and storage performance than SNNU-327. Dynamic breakthrough experiments demonstrate that SNNU-326 can purify CH_4 from C_2H_2/CH_4, C_2H_4/CH_4, C_2H_6/CH_4, and CO_2/CH_4 mixtures with breakthrough interval times of about 40.6, 35.1, 54.2, and 10.2 min g^{-1} (273 K and 1 bar, v/v = 50/50, 2 mL min^{-1}), respectively, which can be comparable with some famous MOF adsorbents. In addition, SNNU-326 shows superior CH_4 storage properties with the total and working uptakes of 154.3 cm^3 (STP) cm^{-3} (80 bar) and 103.4 cm^3 (STP) cm^{-3} (65 bar) at 273 K. The utilization of the heterometallic strategy to rationally design novel MOFs as ideal CH_4 adsorbents with balanced purification and storage abilities is ongoing in our lab.

ASSOCIATED CONTENT

Supporting Information

The Supporting Information is available free. The Supporting Information is available free of charge at https://pubs.acs.org/doi/10.1021/cbe.4c00009.

Experimental details, tables of crystal data, uptake data, IAST selectivities, breakthrough interval time, adsorption capacities, additional crystal structure pictures, PXRD patterns, TGA curves, gas adsorption isotherms, virial and DSLF fitting (PDF)

Crystal data for SNNU-326 (CIF)

Crystal data for SNNU-327 (CIF)

AUTHOR INFORMATION

Corresponding Author

Quan-Guo Zhai – *Key Laboratory of Macromolecular Science of Shaanxi Province, School of Chemistry & Chemical Engineering, Shaanxi Normal University, Xi'an, Shaanxi 710062, China;* orcid.org/0000-0003-1117-4017; Email: zhaiqg@snnu.edu.cn

https://doi.org/10.1021/cbe.4c00009
Chem Bio Eng. 2024, 1, 773–782

Authors

Jiao Lei − *Key Laboratory of Macromolecular Science of Shaanxi Province, School of Chemistry & Chemical Engineering, Shaanxi Normal University, Xi'an, Shaanxi 710062, China; School of Chemical and Chemical Engineering, North University of China, Taiyuan 030051, China*

Zhang-Lei Zhong − *Key Laboratory of Macromolecular Science of Shaanxi Province, School of Chemistry & Chemical Engineering, Shaanxi Normal University, Xi'an, Shaanxi 710062, China*

Wenyu Yuan − *Key Laboratory of Macromolecular Science of Shaanxi Province, School of Chemistry & Chemical Engineering, Shaanxi Normal University, Xi'an, Shaanxi 710062, China*

Peng Zhang − *Key Laboratory of Macromolecular Science of Shaanxi Province, School of Chemistry & Chemical Engineering, Shaanxi Normal University, Xi'an, Shaanxi 710062, China;* orcid.org/0000-0002-1251-8857

Ying Wang − *Key Laboratory of Macromolecular Science of Shaanxi Province, School of Chemistry & Chemical Engineering, Shaanxi Normal University, Xi'an, Shaanxi 710062, China*

Complete contact information is available at: https://pubs.acs.org/10.1021/cbe.4c00009

Author Contributions

#Jiao Lei and Zhang-Lei Zhong contributed equally to this work.

Notes

The authors declare no competing financial interest.

■ ACKNOWLEDGMENTS

This work is financially supported by the National Natural Science Foundation of China (22071140), the Natural Science Foundation of Shaanxi Province (2021JLM-20), the Youth Innovation Team of Shaanxi Universities (2023), and the Fundamental Research Funds for the Central Universities (GK202307009).

■ REFERENCES

(1) Tian, T.; Zeng, Z.; Vulpe, D.; Casco, M. E.; Divitini, G.; Midgley, P. A.; Silvestre-Albero, J.; Tan, J.-C.; Moghadam, P. Z.; Fairen-Jimenez, D. A Sol-gel Monolithic Metal-organic Framework with Enhanced Methane Uptake. *Nat. Mater.* **2018**, *17*, 174−179.

(2) Chen, Z.; Li, P.; Anderson, R.; Wang, X.; Zhang, X.; Robison, L.; Redfern, L. R.; Moribe, S.; Islamoglu, T.; Gómez-Gualdrón, D. A.; Yildirim, T.; Stoddart, J. F.; Farha, O. K. Balancing Volumetric and Gravimetric Uptake in Highly Porous Materials for Clean Energy. *Science* **2020**, *368* (6488), 297−303.

(3) Gándara, F.; Furukawa, H.; Lee, S.; Yaghi, O. M. High Methane Storage Capacity in Aluminum Metal-Organic Frameworks. *J. Am. Chem. Soc.* **2014**, *136* (14), 5271−5274.

(4) Mason, J. A.; Veenstra, M.; Long, J. R. Evaluating Metal-organic Frameworks for Natural Gas Storage. *Chem. Sci.* **2014**, *5*, 32−51.

(5) Connolly, B. M.; Aragones-Anglada, M.; Gandara-Loe, J.; Danaf, N. A.; Lamb, D. C.; Mehta, J. P.; Vulpe, D.; Wuttke, S.; Silvestre-Albero, J.; Moghadam, P. Z.; Wheatley, A. E. H.; Fairen-Jimenez, D. Tuning Porosity in Macroscopic Monolithic Metal-organic Frameworks for Exceptional Natural Gas Storage. *Nat. Commun.* **2019**, *10*, 2345.

(6) Chang, Z.; Jia, X.; Li, T.; Wang, Y.; Li, L. Efficient Separation of C4 Olefins with Fluorinated Anion-pillared Hybrid Ultramicroporous Materials by Gate-opening and Size-sieving Effect. *Sep. Purif. Technol.* **2023**, *318*, 123956.

(7) Xiang, F.; Zhang, H.; Yang, Y.; Li, L.; Que, Z.; Chen, L.; Yuan, Z.; Chen, S.; Yao, Z.; Fu, J.; Xiang, S.; Chen, B.; Zhang, Z. Tetranuclear Cu^{II} Cluster as the Ten Node Building Unit for the Construction of a Metal-Organic Framework for Efficient C_2H_2/CO_2 Separation. *Angew. Chem. Int. Ed.* **2023**, *62*, No. e202300638.

(8) He, Y.; Zhou, W.; Qian, G.; Chen, B. Methane Storage in Metal-organic Frameworks. *Chem. Soc. Rev.* **2014**, *43*, 5657−5678.

(9) Peng, Y.; Krungleviciute, V.; Eryazici, I.; Hupp, J. T.; Farha, O. K.; Yildirim, T. Methane Storage in Metal-Organic Frameworks: Current Records, Surprise Findings, and Challenges. *J. Am. Chem. Soc.* **2013**, *135* (32), 11887−11894.

(10) Rowland, C. A.; Lorzing, G. R.; Gosselin, A. J.; Trump, B. A.; Yap, G. P. A.; Brown, C. M.; Bloch, E. D. Methane Storage in Paddlewheel-Based Porous Coordination Cages. *J. Am. Chem. Soc.* **2018**, *140* (36), 11153−11157.

(11) Tan, K.; Pandey, H.; Wang, H.; Velasco, E.; Wang, K.-Y.; Zhou, H.-C.; Li, J.; Thonhauser, T. Defect Termination in the UiO-66 Family of Metal-Organic Frameworks: The Role of Water and Modulator. *J. Am. Chem. Soc.* **2021**, *143* (17), 6328−6332.

(12) Feng, L.; Day, G. S.; Wang, K.-Y.; Yuan, S.; Zhou, H.-C. Strategies for Pore Engineering in Zirconium Metal-Organic Frameworks. *Chem.* **2020**, *6* (11), 2902−2923.

(13) Feng, L.; Pang, J.; She, P.; Li, J.-L.; Qin, J.-S.; Du, D.-Y.; Zhou, H.-C. Metal-Organic Frameworks Based on Group 3 and 4 Metals. *Adv. Mater.* **2020**, *32* (44), 2004414.

(14) Korman, K. J.; Decker, G. E.; Dworzak, M. R.; Deegan, M. M.; Antonio, A. M.; Taggart, G. A.; Bloch, E. D. Using Low-Pressure Methane Adsorption Isotherms for Higher-Throughput Screening of Methane Storage Materials. *ACS Appl. Mater. Interfaces* **2020**, *12* (36), 40318−40327.

(15) Li, B.; Wen, H.-M.; Zhou, W.; Xu, J. Q.; Chen, B. Porous Metal-Organic Frameworks: Promising Materials for Methane Storage. *Chem.* **2016**, *1* (4), 557−580.

(16) Lin, Y.; Kong, C.; Zhang, Q.; Chen, L. Metal-Organic Frameworks for Carbon Dioxide Capture and Methane Storage. *Adv. Energy Mater.* **2017**, *7* (4), 1601296.

(17) Di, Z.; Liu, C.; Pang, J.; Zou, S.; Ji, Z.; Hu, F.; Chen, C.; Yuan, D.; Hong, M.; Wu, M. A Metal-Organic Framework with Nonpolar Pore Surfaces for the One-Step Acquisition of C_2H_4 from a C_2H_4 and C_2H_6 Mixture. *Angew. Chem. Int. Ed.* **2022**, *61* (42), No. e202210343.

(18) Ma, S.; Wang, X.-S.; Yuan, D.; Zhou, H.-C. A Coordinatively Linked Yb Metal-Organic Framework Demonstrates High Thermal Stability and Uncommon Gas-Adsorption Selectivity. *Angew. Chem. Int. Ed.* **2008**, *47* (22), 4130−4133.

(19) Bloch, E. D.; Queen, W. L.; Krishna, R.; Zadrozny, J. M.; Brown, C. M.; Long, J. R. Hydrocarbon Separations in a Metal-Organic Framework with Open Iron(II) Coordination Sites. *Science* **2012**, *335* (6076), 1606−1610.

(20) Gu, Z.; Li, M.; Chen, C.; Zhang, X.; Luo, C.; Yin, Y.; Su, R.; Zhang, S.; Shen, Y.; Fu, Y.; Zhang, W.; Huo, F. Water-Assisted Hydrogen Spillover in Pt Nanoparticle-based Metal-organic Framework Composites. *Nat. Commun.* **2023**, *14*, 5836.

(21) Ullah, S.; Jensen, S.; Liu, Y.; Tan, K.; Drake, H.; Zhang, G.; Huang, J.; Klimeš, J.; Driscoll, D. M.; Hermann, R. P.; Zhou, H.-C.; Li, J.; Thonhauser, T. Magnetically Induced Binary Ferrocene with Oxidized Iron. *J. Am. Chem. So.c* **2023**, *145* (32), 18029−18035.

(22) Li, H.; Eddaoudi, M.; O'Keeffe, M.; Yaghi, O. M. Design and Synthesis of an Exceptionally Stable and Highly Porous Metal-organic Framework. *Nature* **1999**, *402*, 276−279.

(23) Tu, B.; Pang, Q.; Wu, D.; Song, Y.; Weng, L.; Li, Q. Ordered Vacancies and Their Chemistry in Metal-Organic Frameworks. *J. Am. Chem. Soc.* **2014**, *136* (41), 14465−14471.

(24) Ma, S.; Zhou, H.-C. A Metal-Organic Framework with Entatic Metal Centers Exhibiting High Gas Adsorption Affinity. *J. Am. Chem. Soc.* **2006**, *128* (36), 11734−11735.

(25) Lei, J.; Zhang, P.; Xue, Y.-Y.; Xu, J.; Li, H.-P.; Lv, H.-J.; Wang, Y.; Li, S.-N.; Zhai, Q.-G. Design of Ultra-stable Yttrium-organic Framework Adsorbents for Efficient Methane Purification and Storage. *Sep. Purif. Technol.* **2022**, *283*, 120211.

(26) Blake, A. J.; Brooks, N. R.; Champness, N. R.; Crew, M.; Deveson, A.; Fenske, D.; Gregory, D. H.; Hanton, L. R.; Hubberstey, P.; Schröder, M. Topological Isomerism in Coordination Polymers. *Chem. Commun.* **2001**, 1432−1433.
(27) Li, H.-P.; Dou, Z.-D.; Xiao, Y.; Fan, G.-J.; Pan, D.-C.; Hu, M.-C.; Zhai, Q.-G. Rational Regulation of Acetylene Adsorption and Separation for Ultra-microporous Copper-1,2,4-triazolate Frameworks by Halogen Hydrogen Bonds. *Nanoscale* **2022**, *14*, 18200−18208.
(28) Wang, D.; Liu, Z.; Xu, L.; Li, C.; Zhao, D.; Ge, G.; Wang, Z.; Lin, J. A Heterometallic Metal-Organic Framework Based on Multi-nuclear Clusters Exhibiting High Stability and Selective Gas Adsorption. *Dalton Trans.* **2019**, *48*, 278−284.
(29) Wang, H.-H.; Jia, L.-N.; Hou, L.; Shi, W.-j.; Zhu, Z.; Wang, Y.-Y. A New Porous MOF with Two Uncommon Metal-Carboxylate-Pyrazolate Clusters and High CO_2/N_2 Selectivity. *Inorg. Chem.* **2015**, *54* (4), 1841−1846.
(30) Hou, L.; Lin, Y.-Y.; Chen, X.-M. Porous Metal-Organic Framework Based on μ_4-oxo Tetrazinc Clusters: Sorption and Guest-Dependent Luminescent Properties. *Inorg. Chem.* **2008**, *47* (4), 1346−1351.
(31) Tonigold, M.; Lu, Y.; Mavrandonakis, A.; Puls, A.; Staudt, R.; Möllmer, J.; Sauer, J.; Volkmer, D. Pyrazolate-Based Cobalt(II)-Containing Metal-Organic Frameworks in Heterogeneous Catalytic Oxidation Reactions: Elucidating the Role of Entatic States for Biomimetic Oxidation Processes. *Chem.—Eur. J.* **2011**, *17* (31), 8671−8695.
(32) Duan, X.; Lv, R.; Ji, Z.; Li, B.; Cui, Y.; Yang, Y.; Qian, G. Highly Stable Y(iii)-based Metal Organic Framework with Two Molecular Building Block for Selective Adsorption of C_2H_2 and CO_2 over CH_4. *Inorg. Chem. Front.* **2018**, *5*, 1193−1198.
(33) Banerjee, R.; Furukawa, H.; Britt, D.; Knobler, C.; O'Keeffe, M.; Yaghi, O. M. Control of Pore Size and Functionality in Isoreticular Zeolitic Imidazolate Frameworks and their Carbon Dioxide Selective Capture Properties. *J. Am. Chem. Soc.* **2009**, *131* (11), 3875−3877.
(34) Burd, S. D.; Ma, S.; Perman, J. A.; Sikora, B. J.; Snurr, R. Q.; Thallapally, P. K.; Tian, J.; Wojtas, L.; Zaworotko, M. J. Highly Selective Carbon Dioxide Uptake by $[Cu(bpy\text{-}n)_2(SiF_6)]$ (bpy-1 = 4,4′-Bipyridine; bpy-2 = 1,2-Bis(4-pyridyl)ethene). *J. Am. Chem. Soc.* **2012**, *134* (8), 3663−3666.
(35) Simmons, J. M.; Wu, H.; Zhou, W.; Yildirim, T. Carbon Capture in Metal-Organic Frameworks——A Comparative Study. *Energy Environ. Sci.* **2011**, *4*, 2177−2185.
(36) Wang, Y.; He, M.; Gao, X.; Li, S.; Xiong, S.; Krishna, R.; He, Y. Exploring the Effect of Ligand-Originated MOF Isomerism and Methoxy Group Functionalization on Selective Acetylene/Methane and Carbon Dioxide/Methane Adsorption Properties in Two NbO-Type MOFs. *ACS Appl. Mater. Interfaces* **2018**, *10* (24), 20559−20568.
(37) Li, Q.; Wu, N.; Li, J.; Wu, D.; Li, Y. Amino-Functionalized Water-Stable Metal-Organic Framework for Enhanced C_2H_2/CH_4 Separation Performance. *Inorg. Chem.* **2020**, *59* (5), 2631−2635.
(38) Chen, Y.; Qiao, Z.; Lv, D.; Wu, H.; Shi, R.; Xia, Q.; Wang, H.; Zhou, J.; Li, Z. Selective Adsorption of Light Alkanes on a Highly Robust Indium Based Metal-Organic Framework. *Ind. Eng. Chem. Res.* **2017**, *56* (15), 4488−4495.
(39) Liang, C.-C.; Shi, Z.-L.; He, C.-T.; Tan, J.; Zhou, H.-D.; Zhou, H.-L.; Lee, Y.; Zhang, Y.-B. Engineering of Pore Geometry for Ultrahigh Capacity Methane Storage in Mesoporous Metal-Organic Frameworks. *J. Am. Chem. Soc.* **2017**, *139* (38), 13300−13303.
(40) Llewellyn, P. L.; Bourrelly, S.; Serre, C.; Vimont, A.; Daturi, M.; Hamon, L.; De Weireld, G.; Chang, J.-S.; Hong, D.-Y.; Kyu Hwang, Y.; Hwa Jhung, S.; Ferey, G. High Uptakes of CO_2 and CH_4 in Mesoporous Metal-Organic Frameworks MIL-100 and MIL-101. *Langmuir* **2008**, *24* (14), 7245−7250.
(41) Yan, Y.; Yang, S.; Blake, A. J.; Lewis, W.; Poirier, E.; Barnett, S. A.; Champness, N. R.; Schröder, M. A Mesoporous Metal-organic Framework Constructed from a Nanosized C_3-symmetric Linker and $[Cu_{24}(isophthalate)_{24}]$ Cuboctahedra. *Chem. Commun.* **2011**, *47*, 9995−9997.
(42) Furukawa, H.; Ko, N.; Go, Y. B.; Aratani, N.; Choi, S. B.; Choi, E.; Yazaydin, A. Ö.; Snurr, R. Q.; O'Keeffe, M.; Kim, J.; Yaghi, O. M. Ultrahigh Porosity in Metal-Organic Frameworks. *Science* **2010**, *329* (5990), 424−428.

https://doi.org/10.1021/cbe.4c00009
Chem Bio Eng. 2024, 1, 773−782